Theor Chem Acc (2011) 128:341–348
DOI 10.1007/s00214-010-0860-1

REGULAR ARTICLE

Unimolecular decomposition mechanism of vinyl alcohol by computational study

Ju-Xiang Shao · Chun-Ming Gong · Xiang-Yuan Li · Jun Li

Received: 15 June 2010 / Accepted: 15 November 2010 / Published online: 14 December 2010

Abstract Although vinyl alcohol(CH_2=CHOH)molecule was found to be an important intermediate in the combustion flames of hydrocarbon (Taatjes et al. in Science 308:1887, 2005), the removal mechanism of vinyl alcohol has not been established yet. The removal mechanism is critical to characterize the kinetics behavior of hydrocarbon in combustion chemistry and to develop the chemical models of hydrocarbon oxidation. In this work, the potential energy surface for the unimolecular decomposition of *syn*-CH_2=CHOH reaction has been first studied by ab initio. The kinetics and product branching ratios for the decomposition reaction are evaluated by Variflex code in the temperature range of 500–3,000 K at 0.1, 1.0, and 100.0 atmosphere pressure. The results show that the formation of CH_3 + CHO via the CH_3CHO intermediate is dominant in the decomposition reaction and its branching ratios at 0.1, 1.0, and 100.0 atm are more than 99.90, 99.30, and 89.20%, respectively, through the whole temperature range investigated.

Keywords Vinyl alcohol · Unimolecular decomposition · Mechanism · Rate constant

J.-X. Shao · C.-M. Gong · X.-Y. Li (✉) · J. Li
College of Chemical Engineering, Sichuan University, 610065 Chengdu, People's Republic of China
e-mail: xyli@scu.edu.cn

J.-X. Shao
Computational Physics Key Laboratory of Sichuan Province, Yibin University, 644000 Yibin, Sichuan Province, People's Republic of China

1 Introduction

Although in 1880 enols were first postulated by Erlenmeyer [1] as transient chemical intermediates, until 1976, vinyl alcohol (CH_2=CHOH, ethenol), the simplest enol, was observed in a gas phase [2]. Since then, enols have been the subject of numerous experimental and theoretical studies [2–15]. In 2003, vinyl alcohol was observed by Cool et al. in a fuel-rich ethene combustion flame for the first time [9], and then in 2005, Taatjes et al. [10] reported that the flames fueled by rich propene, propyne, allene, benzene, ethanol, etc., also showed substantial contributions from vinyl alcohol. The traditional hydrocarbon combustion chemistry assumed C_2H_4O molecules observed in flames as CH_3–CH=O (acetaldehyde, ethanal) or c-C_2H_4O (ethylene oxide, oxirane). However, Taatjes et al. [10] discovered that there should be different mechanisms in the formation of CH_2=CHOH and CH_3–CH=O tautomer in the combustion flames of hydrocarbon. The theoretical studies accomplished by Yamada et al. [11] and Hippler et al. [12] with ab initio method revealed that the reaction of OH radical with ethene could produce the product of vinyl alcohol. The experiment carried out by Taatjes et al. [13] demonstrated that reaction of OH with alkene was a key source of enols in the preheat zone of low-pressure flames, and Cool et al. [9] in the experiment study found that OH addition to hydrocarbon radicals as well as dehydrogenation of alcohol might form vinyl alcohol. Although it is evident that vinyl alcohol is present in substantial concentrations in a wide range of hydrocarbon combustion flames, the detailed theoretical analyses of vinyl alcohol removal reactions for reliable modeling of enol chemistry over a wide range of combustion conditions have still been unavailable [13]. Theoretical investigation into removal reactions for vinyl

alcohol would be very helpful in explaining the chemistry of enols in hydrocarbon flames.

In previous studies, Saito [2] and Rodler et al. [14] investigated the structure of vinyl alcohol molecule by the molecular microwave spectrum. Their experimental results revealed that vinyl alcohol was planar and had the *syn* form. Tureček et al. [15] studied thermochemistry of vinyl alcohol and its cation radical at the G2 (MP2) ab initio level. They proposed that *syn*-planar conformation was more thermodynamically stable for vinyl alcohol in the gas phase than the *anti*-planar conformation.

In spite of a wealth of data on vinyl alcohol structure and thermochemistry [2, 14–16], there remain several unresolved problems of a fundamental nature. First, although vinyl alcohol as an intermediate was observed in the hydrocarbon combustion flames [10], the kinetics and mechanism for its decomposition reaction over a wide range combustion condition, which assist in explaining the stability of vinyl alcohol in the neutral gas phase, have not been yet investigated. Second, the rate constants of the decomposition of *syn*-vinyl alcohol and the product branching ratios of each decomposition channel under the wide temperature combustion condition have not been described in detail. As is known to us, reliable determination of the decomposition mechanisms and the branching rate constants are critical to characterize the kinetics behavior of *syn*-vinyl alcohol in combustion chemistry and to develop the chemical models of hydrocarbon oxidation.

Under combustion conditions, the unimolecular decomposition of *syn*-CH_2=CHOH may occur through many energetically accessible product channels:

$$\textit{syn}\text{-}CH_2CHOH \xrightarrow{k_1} CH_2COH + H \quad (1)$$

$$\xrightarrow{k_2} CH_2C + H_2O \quad (2)$$

$$\xrightarrow{k_3} CHCH + H_2O \quad (3)$$

$$\xrightarrow{k_4} CH_3CHO \rightarrow CH_3 + CHO \quad (4)$$

$$\xrightarrow{k_5} CH_3COH \quad (5)$$

$$\xrightarrow{k_6} CH_2CHO + H \quad (6)$$

$$\xrightarrow{k_7} CHCHOH + H \quad (7)$$

$$\xrightarrow{k_8} CH_2CH + OH \quad (8)$$

The energies of these reactions are calculated at ab initio level. Meanwhile, the rate constants and products branching ratios are reported herein for high-temperature combustion modeling applications. Few data from experiment and computation are available on these reaction channels in neutral gas-phase combustion chemistry.

2 Computational methods

2.1 Potential energy surface calculations

For the decomposition of *syn*-vinyl alcohol, it is critical to generate an accurate and reliable potential energy surface (PES) in order to predict reliable reaction rate constants and products branching ratios. The equilibrium geometries of the reactant, transition states, and products are optimized by the hybrid density functional (B3LYP) method (Becke's three-parameter nonlocal exchange functional [17, 18] with the nonlocal correlation functional of Lee, Yang, and Parr [19]) with the 6-311G(d, p) basis set [20]. Andersson et al. [21] by calculating the molecular set of 125 molecules for low-frequency vibrations and the set of 40 molecules for zero-point energies proposed that for B3LYP/6-311G(d,p) level, the scale factors are 0.9679 for vibrational frequencies and 0.9877 for zero-point vibrational energies. In this work, vibrational frequencies and zero-point energy (ZPE) of all species are also calculated at this level and scaled by scale factor of 0.9679 and 0.9877, respectively, as recommended by Andersson et al. [21]. These values are employed for characterization of the nature of stationary points and rate constant calculations. All the stationary points are considered as local minima, i.e., there is no imaginary frequency for reactant and products, and one and only one imaginary frequency for transition states. The intrinsic reaction coordinate (IRC) method [22] is utilized to validate the connection between the transition state and the reactant or product. For more accurate evaluation of the energies of the reaction, the CCSD(T)/6-311 + G(3df,2p) [23] method is employed to obtain the single-point energy based on the optimized geometries from the B3LYP/6-311G(d,p) level. All quantum chemistry calculations are performed by the Gaussian 03 package [24].

2.2 Rate constant calculations

The rate constants for the key products are computed with variational transition state theory (VTST) and Rice–Ramsperger–Kassel–Marcus (RRKM) theory using the Variflex codes by Klippenstein and co-workers [25]. The RRKM theory expression for the unimolecular dissociation rate constant at the *E*- and *J*-resolved levels, $K(E, J)$, may be written as

$$K(E,J) = \frac{N(E,J)}{h\rho(E,J)}$$

where $N(E, J)$ is the sum of states of the transition state to energy E with angular momentum J, and $\rho(E, J)$ is the density of states of the reactants at the specified energy and angular momentum, and h is Planck's constant. $N(E, J)$ and $\rho(E, J)$ were counted with a grain size of 1 cm^{-1} using the

Beyer-Swinehart-Stein-Rabinovith algorithm [26, 27]. The pressure dependence of rate constants is treated by one-dimensional (1D) master equation calculations using the Boltzmann probability of the complex for the J distribution. The master equation is solved by eigenvalue-solver-based approach for the dissociation processes [28, 29]. The details of the formulation of the master equation and methodology of solution used in Variflex are described in detail elsewhere [30–34]. So as to accomplish convergence in the integration over the energy range, an energy grain size of 100 cm^{-1} is used. This grain size provides numerically converged results for the conditions investigated, with the energy spanning the range from $-37{,}808.0$ cm^{-1} below to 42,192.0 cm^{-1} above the threshold forming $CH_2COH + H$. The total angular momentum J covers the range from 1 to 251 with a step length 10 for the E-, J-resolved calculation. For the reaction without barrier transition state, the Morse potential, $E(R) = D_e[1 - \exp\{-\beta(R - R_e)\}]^2$, is used to represent the potential energy along the individual reaction coordinate, in which R is the reaction coordinate (i.e., the distance between the two bonding atoms; C–H, O–H or C–C in this work), D_e is the bond dissociation energy, R_e is the equilibrium value of R, $\beta = (f_e/2D_e)^{1/2}$, and f_e is the force constant of the bond at the minimum of the potential well. For the reaction with tight transition state, the numbers of states are evaluated according to the rigid-rotor harmonic oscillator assumption. The energetic and other parameters, such as reaction barriers, rotational constants and vibrational frequencies from the ab initio calculations, are used in the rate constant calculation. To facilitate the use of the reaction rate constants for chemical kinetics modeling, we fit all rate constants in the temperature range from 500 to 3,000 K and in the pressure range from 0.1 to 100.0 atm to a modified three-parameter Arrhenius expression

$$K(T) = AT^n \exp\left(-\frac{E_a}{RT}\right)$$

This formulation leads to a better fit than the ordinary Arrhenius expression, but the parameters may have little physical interpretation.

3 Results and discussion

3.1 Potential energy surface of the system and reaction mechanism

The key product channels for the decomposition of *syn*-vinyl alcohol mentioned previously will be only considered. At the B3LYP/6-311G(d,p) level, the optimized geometries of the reactant, transition states, and products are showed in Fig. 1 including the characteristic bond distances and angles. Figure 2 shows the potential energy surface obtained at the CCSD(T)/6-311 + G(3df,2p) level. The vibrational frequencies and rotational constants of all species used in the rate constant calculations are presented in Table 1. The reaction paths for the channels (1)–(6) shown in Fig. 2 will be discussed sequentially in the following sections, whereas the higher energy processes (7) and (8) will not be included in our rate constant calculation, just the same treatment as proposed by Zhou et al. [35] and Park co-workers [36]. All reaction channels considered here are indeed the one-step mechanisms, except channel (4).

As shown in Fig. 1, it is seen that the *syn*-vinyl alcohol may isomerize to the *anti*-vinyl alcohol configuration through the transition state (TS1). The transition state lies above *syn*-vinyl alcohol by 4.60 kcal/mol. The energy of *anti*-form lies above that of *syn*-form by 0.945 kcal/mol, which is in agreement with the previous experimental and theoretical results [2, 14, 37–39]. It can be seen that vinyl alcohol prefers the more stable *syn*-conformation in the gas phase. Therefore, we only take the decomposition of the *syn*-conformation into account in the following discussion.

3.1.1 CH_2COH +H channel

For the fragmentation reaction producing $CH_2COH + H$, it is a barrierless path. On account of the absence of a well-defined transition state, its dissociation potential function is computed variationally to cover a range of C–H bond separations from the equilibrium value 1.084–6.284 Å with an interval of 0.2 Å. At the B3LYP/6-311++G(d,p) level, we optimize every structure at each interval of the C–H bond separation by freezing the C–H bond. In this manner, a smooth and reasonable potential curve in terms of total energy at each point along the reaction path is obtained and employed to evaluate the Morse potential energy function mentioned earlier. The potential energy function, $E(R)$, is obtained with $\beta = 2.130$ $Å^{-1}$, and $R_e = 1.084$ Å, and the predicted dissociation energy, 108.0 kcal/mol, is in good agreement with the calculation value (108.1 kcal/mol) at the CCSD(T)/6-311 + G(3df,2p) level and the previous value predicted (109.1 kcal/mol) by Silva et al. [16] using enthalpies of formation. The potential for the dissociation process is used in subsequent rate constant calculations based on the RRKM theory.

3.1.2 CH_2C +H_2O channel

This is a dehydration process. As shown in Fig. 1, in this channel, the H_2O elimination process involves the H atom in the CH group via a three-member-ring transition state, TS21, in which the breaking C–H and C–O bonds in TS21 are 0.151 and 0.509 Å longer than those in *syn*-vinyl alcohol, respectively. H atom from CH group is closed to O

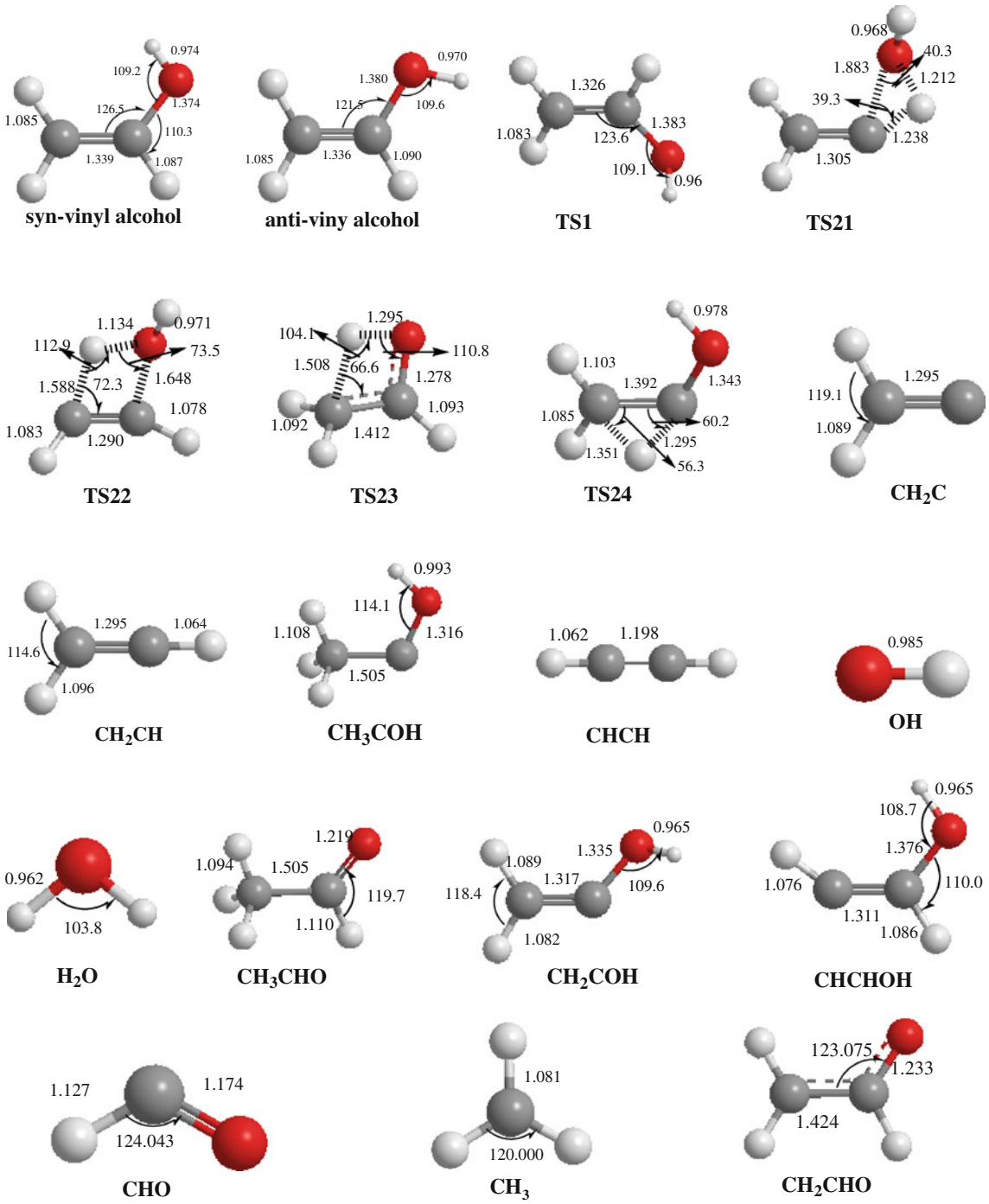

Fig. 1 Optimized geometries of the reactant, transition states, and products involved in the *syn*-vinyl alcohol decomposition reactions at the B3LYP/6-311(d,p) level. The bond lengths are in angstrom, and the angles are in degree

atom in OH group with a value of 39.3° for band angle OCH, in which the band angle is 71.0° less than that in *syn*-vinyl alcohol. TS21 with the imaginary frequency of 1,335*i* cm^{-1} represents a well-defined transition state. The result of IRC calculation confirms that TS21 connects the reactant and the products $CH_2C + H_2O$, in which TS21 lies above *syn*-vinyl alcohol by 81.0 kcal/mol.

3.1.3 CHCH +H_2O channel

This is also a dehydration process. As presented in Fig. 1, H_2O elimination from *syn*-vinyl alcohol occurs via a planar four-member-ring transition state, TS22, in which the out-of-ring H atom bonded to O atom is largely bent away from the HCCO plane, with a value of 104.8° for dihedral angle

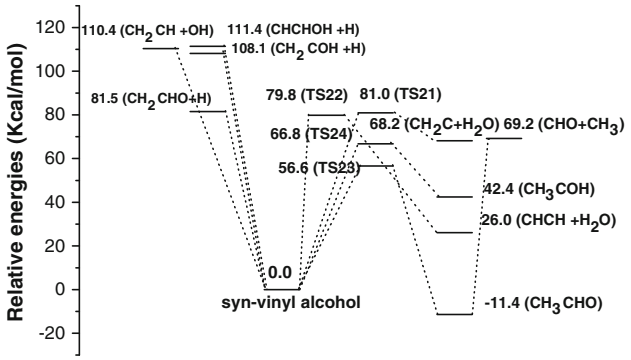

Fig. 2 Potential energy diagram for dissociation of *syn*-vinyl alcohol at the CCSD(T)/6-311 + G(3*df*,2*p*)//B3LYP/6-311G(*d*,*p*) with zero-point energy correction obtained from B3LYP/6-311G(*d*,*p*) results

HOCC. The breaking C–H and C–O bonds in TS22 are 0.493 and 0.374 Å longer than those in *syn*-vinyl alcohol. TS22 with the imaginary frequency of 1,337*i* cm^{-1} shows a well-defined transition state. TS22 lies above *syn*-vinyl alcohol by 79.8 kcal/mol and leads to the formation of CHCH $+H_2O$.

3.1.4 $CH_3CHO \rightarrow CH_3 + CHO$ channel

This reaction channel consists of two steps. The first step is to start from the isomerization of *syn*-vinyl alcohol to acetaldehyde (CH_3CHO) by the rearrangement of hydrogen atom. As shown in Fig. 1, the H atom in the OH group in *syn*-vinyl alcohol can migrate toward the C atom in the CH_2 group to produce CH_3CHO via a four-member-ring transition state, TS23. The breaking O–H in TS23 is 0.321 Å longer than that in *syn*-vinyl alcohol. The height of barrier this step is 56.6 kcal/mol, which is consistent with the previous theoretical values of 56.2 kcal/mol [8], 55.9 kcal/mol [16] from G1 and CBS-APNO level, respectively. Then the second step, the unimolecular decomposition of CH_3CHO which has been studied experimentally and theoretically by other groups [40–47], is also taken into account. Although the previous literatures proposed that decomposition of CH_3CHO might form $CH_3 + CHO$, $CH_4 + CO$, $CH_2CO + H_2$, $CH_2CHO + H$, and/or $CH_3CO + H$ products, the experimental studies [40–42] on the thermal decomposition of CH_3CHO were presumed to yield CH_3 +CHO via C–C bond scission, i.e., $CH_3CHO \rightarrow CH_3 + CHO$. The theoretical study from Harding et al. [47] was considered that the major productions of decomposition of CH_3CHO are CH_3 and CHO. So, we also consider CH_3 and CHO as the products of thermal decomposition of CH_3CHO in this work. The potential energies of the dissociation process from CH_3CHO to $CH_3 + CHO$ are calculated by geometry optimization at different fixed H_3C–CHO separations covering from the equilibrium value 1.504–7.104 Å with an interval of 0.2 Å. The calculated energies from the B3LYP/6-311 ++G(d,p) level are fitted to the Morse potential mentioned previously with $D_e = 80.6$ kcal/mol, $\beta = 2.138$ $Å^{-1}$, and $R_e = 1.504$ Å, in which the C–C bond dissociation energy of CH_3CHO into $CH_3 + HCO$, D_e, is in good agreement with the theoretical value of 81.9 kcal/mol [42] at QCISD(T)/6-31G(d) level. The potential parameters for the dissociation process are used in RRKM calculations.

Table 1 Vibrational frequencies and rotational constants (*B*) for the species involved in the *syn*-vinyl alcohol decomposition reaction computed at the B3LYP/6-311G(d, p) level

Species	*B* (MHz)	Frequencies (cm^{-1})[a]
syn-vinyl alcohol	60,917, 10,531, 8,978	461, 476, 691, 797, 930, 966, 1,090, 1,284, 1,316, 1,402, 1,648, 3,038, 3,082, 3,135, 3,681
anti-vinyl alcohol	64,241,10,428, 8,972	246, 467, 694, 817, 926, 946, 1,108, 1,250, 1,306, 1,391, 1,677,3,032, 3,059, 3,148, 3,744
TS1	59,518,10,359, 9,060	419*i*, 474, 674, 880, 917, 952, 1,104, 1,202, 1,297, 1,376, 1,647, 3,015, 3,047, 3,133, 3,704
TS21	51,759, 8,253, 7,291	1,335*i*, 291, 304, 490, 604, 790, 846, 913, 1,229, 1,285, 1,591, 2,174, 3,024, 3,108, 3,655
TS22	44,682,11,095, 9,123	1,337*i*, 427, 525, 658, 736, 829, 855, 956, 1,117, 1,346, 1,585, 1,850, 3,097, 3,151, 3,600
TS23	48,843, 12,289, 10,234	2,111*i*, 552, 623, 766, 937, 1,029, 1,106, 1,161, 1,255, 1,416, 1,499, 1,810, 2,984, 3,004, 3,067
TS24	57,741, 10,814, 9,469	1,404*i*, 483, 611, 675, 923, 1,000, 1,082, 1,262, 1,305, 1,348, 1,460, 2,070, 2,848, 3,088, 3,412
CH_3CHO	57,203, 10,132, 9,090	155, 492, 752, 854, 1,089, 1,099, 1,331, 1,380, 1,414, 1,424, 1,765, 2,765, 2,925, 2,978, 3,036
CH_3COH	52,194, 10,614, 9,319	142, 519, 722, 878, 951, 1,022, 1,289, 1,313, 1,326, 1,383, 1,419, 2,792, 2,961, 2,983, 3,206
CHCH	35,652	618, 744, 744, 2,004, 3,316, 3,415
CH_2C	284,566, 39,677, 34,822	332, 728, 1,173, 1,655, 3,013, 3,089
CH_2CHO	67,355, 11,456, 9,791	436, 489, 732, 944, 948, 1,114, 1,352, 1,423, 1,503, 2,835, 3,037, 3,149
H_2O	38,489, 21,001, 13,587	1,585, 3,690, 3,784
CH_3	286,280, 286,280, 143,140	490, 1,358, 1,358, 3,003, 3,176, 3,176
CHO	707,540, 44,968, 42,281	1,075, 1,879, 2,537

[a] Values are scaled by 0.9679, *i* denotes the imaginary frequency

3.1.5 CH_3COH channel

This channel is also isomerization process. The H atom in the CH group can migrate toward the C atom in the CH_2 group to produce CH_3COH (1-hydroxyethylidene) via a three-member-ring transition state, TS24, with the imaginary frequency of 1,404*i* cm^{-1}, in which the breaking C–H is 0.208 Å longer than that in *syn*-vinyl alcohol. H atom from CH group is closed to C atom in CH_2 group, with a value of 60.2° for band angle CCH, in which the band angle is 63.0° less than that in *syn*-vinyl alcohol. TS24 lies up to 66.8 kcal/mol above *syn*-vinyl alcohol, which is close to the theoretical value of 63.6 kcal/mol predicted by Smith et al. [8]. The result of IRC calculation confirms that TS24 connects the reactant and the CH_3COH product.

3.1.6 CH_2CHO +H channel

Similar to channel (1), the reaction occurs without a well-defined transition state. The $CH_2CHO + H$ dissociation potential function is computed variationally to cover the range of O–H from 0.965 to 5.565 Å. At the B3LYP/6-311 ++G(d,p) level, we carefully optimize every structure at each interval of the O–H bond separation by freezing the O–H bond, and a smooth and reasonable potential curve in terms of total energy at each point along the fission reaction path is found. The Morse potential energy function mentioned earlier is obtained with $D_e = 87.8$ kcal/mol, $\beta = 3.268$ $Å^{-1}$, and $R_e = 0.965$ Å. The predicted dissociation energy, 87.8 kcal/mol, is close to the literature value (85.2 kcal/mol) estimated by Silva et al. [16] with enthalpies of formation.

3.2 Rate constant and product branching ratio

3.2.1 Rate constant

For the decomposition of *syn*-vinyl alcohol reactions, as mentioned previously, there are eight possible channels. However, channels (7) and (8) with bond dissociation energies of 111.4 and 110.4 kcal/mol, respectively, are less important in the thermal decomposition reaction. Therefore, the rate constants for competitive channels (1)–(6) are computed with VTST and RRKM theory using the Variflex code [25] based on the PES and mechanisms presented in Sect. 3.1, in the temperature range of 500–3,000 K and the pressure range from 0.1 to 100 atm, in which N_2 bath gas is considered the realistic combustion of hydrocarbon fuel in engine. The behavior of energy transfer is assumed to be induced by weak molecular collision, and the frequency of collision is derived from the Lennard–Jones (L-J) potential [48, 49], $V(\text{pair}) = 4\varepsilon[(\sigma/r)^{12} - (\sigma/r)^6]$, where r is the center-of-mass separation between N_2 and CH_2CHOH, ε is the maximum depth of the potential well, and σ is the separation at which $V(\text{pair}) = 0$. The L-J parameters for CH_2CHOH and N_2 employed in the calculation, $\sigma = 4.791$ and 3.798 Å as well as $\varepsilon/k_B = 331.7$ and 82.0 K, respectively, are taken from the literatures [50, 51], which are employed to evaluate the L-J parameters for each collision pair using the approximations $\sigma_{12} = (\sigma_1 + \sigma_2)/2$ and $\varepsilon_{12} = (\varepsilon_1\varepsilon_2)^{1/2}$. The energy transfer per downward collision, $\langle \Delta E_{down} \rangle$, is assumed to be 200 cm^{-1} in N_2 bath gas in the calculation [52]. The energies given in Fig. 2 and the rotational constants and the vibrational frequencies listed in Table 1 are utilized to compute the rate constants. The quantum tunneling effects are included in the related cases with the Eckart tunneling model [53]. The number of states and the density of states are obtained from rigid-rotor harmonic oscillator assumptions [19] for all but the syn-$CH_2CHO\cdots H$ complex torsional mode, for which a one-dimensional hindered rotor treatment is employed. The torsional mode links to the anti-conformer by a hindered rotation of TS1 with the barrier of 4.60 kcal/mol. Moreover, the Morse potential given above, the L-J potential, and the anisotropic potential are added together to construct the final potential for the variational rate constant calculation, in which a potential anisotropy forms, assuming a bonding potential that is cylindrically symmetric with respect to each fragment.

The calculated various channels' individual rate constants for *syn*-vinyl alcohol decomposition at different temperatures and pressures are summarized in Table 2. The Arrhenius plots showing temperature dependence of the

Table 2 Rate constants (s^{-1}) fitted at different pressures

0.1 atm	1.0 atm	100.0 atm
k_1 6.78×10^{-10} $T^{-0.48}$ exp(−30,638/*T*)	9.10×10^{-17} $T^{1.50}$ exp(−19,369/*T*)	2.43×10^{44} $T^{-10.21}$ exp(−53,343/*T*)
k_2 2.57×10^{61} $T^{-16.70}$ exp(−45,323/*T*)	3.26×10^{63} $T^{-16.05}$ exp(−48,099/*T*)	4.07×10^{50} $T^{-10.95}$ exp(−48,862/*T*)
k_3 9.85×10^{60} $T^{-16.89}$ exp(−45,598/*T*)	1.24×10^{63} $T^{-16.19}$ exp(−48,364/*T*)	2.40×10^{50} $T^{-11.09}$ exp(−49,266/*T*)
k_4 7.42×10^{46} $T^{-10.56}$ exp(−33,931/*T*)	4.42×10^{42} $T^{-9.09}$ exp(−33,754/*T*)	2.90×10^{27} $T^{-4.35}$ exp(−31,008/*T*)
k_5 2.35×10^{56} $T^{-13.88}$ exp(−40,393/*T*)	4.09×10^{54} $T^{-12.84}$ exp(−41,552/*T*)	3.16×10^{38} $T^{-7.55}$ exp(−39,575/*T*)
K_6 4.16×10^{65} $T^{-17.67}$ exp(−47,156/*T*)	7.71×10^{66} $T^{-16.74}$ exp(−49,327/*T*)	4.92×10^{54} $T^{-11.75}$ exp(−50,262/*T*)

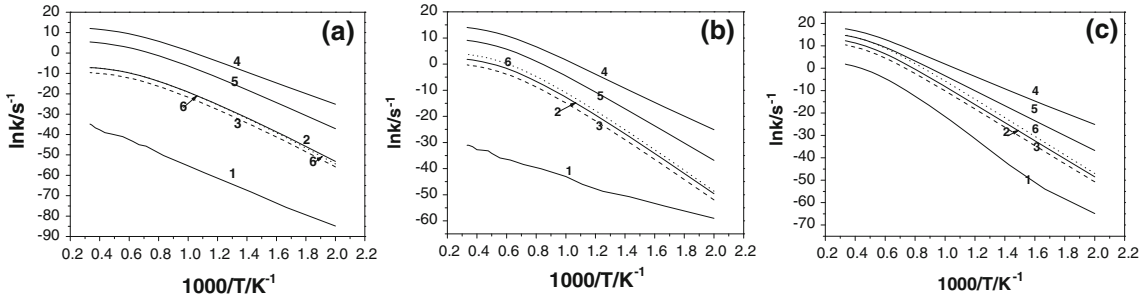

Fig. 3 Temperature dependence of rate constants at **a** 0.1 atm, **b** 1.0 atm, and **c** 100.0 atm for decomposition reactions (1)–(6). The numbers in the figure correspond to each reaction channel given in the introduction

rate constants are presented in Fig. 3a at 0.1 atm, in Fig. 3b at 1.0 atm, and in Fig. 3c at 100.0 atm pressure. As shown in Fig. 3a, at 0.1 atm, the major reactions are channels (4) and (5), but the rate constant k_4 is larger than k_5 in the whole temperature range. For the trivial channels, the inequality $k_2 > k_3 > k_1$ keeps and k_6 and k_2 almost superposes. At 1.0 atm [see Fig. 3 (b)], the magnitude sequence of k_1–k_6 is similar to that predicted at 0.1 atm. Channel (4) is an important reaction, and k_4 is larger than the other five channels. For channels (2), (3), and (6), their rate constants, k_2, k_3, and k_6, are very close, and k_6 is slightly larger than k_2 throughout the whole temperature range, because in the energy diagram of Fig. 2, the dissociation energy of channel (6) is only higher than energy barrier of TS21 for channel (2) by 0.5 kcal/mol, and the latter is only higher than that of TS22 for channel (3) by 1.2 kcal/mol. The relative magnitudes of the rate constants at different temperatures shown in Fig. 3b may be attributed to the combined effects of their barriers and transition state structures (i.e., the enthalpies and entropies of the TS's). At 100.0 atm [see Fig. 3c], the magnitude sequence of k_1–k_6 is similar to that predicted at 1.0 atm, but k_6 is very closer to k_5 than those predicted at 1.0 atm pressure, especially in the high temperature range, in which it is found that the curves of rate constant for k_6 and k_5 almost superposes beyond 1,600 k. It is readily seen that at the three different pressures, the lowest energy barrier of the process from *syn*-vinyl alcohol to acetaldehyde (CH_3–CH = O) in channel (4) is dominant due to its relatively low-energy barrier. Formation of CH_3 and HCO products from acetaldehyde [channel (4)] is more important than the other products. On the other hand, k_1, as expected, becomes the lowest one in the temperature and pressure range investigated, because of its high-energy barrier of 108.1 kcal/mol.

For practical applications in hydrocarbon combustion flames, the rate constants from variflex for channels (1)–(6) at 500–3,000 K at different pressures with N_2 as the third body are fitted to the modified three-parameter Arrhenius expression given above and are listed in Table 2.

3.2.2 Product branching ratio

For the unimolecular decomposition of *syn*-CH_2=CHOH reaction, the temperature and pressure dependence of products branching ratios is discussed. In whole temperature and pressure range investigated, the branching ratios of CH_2COH + H [channel (1)], CH_2C +H_2O [(channel (2)], and CHCH +H_2O [channel (3)] are negligibly small, with a maximum value less than 0.43%. At 0.1 atm, branching ratio for the formation of CH_3 + CHO via intermediate CH_3CHO [channel (4)] is predicted to be more than 99.90% through the whole temperature range. At 1.0 atm, the magnitude sequence of product branching ratio for different channel is similar to that predicted at 0.1 atm. Channel (4) is also major reaction, and its branching ratio is more than 99.3%. At 100 atm, channel (4) is also dominant in the decomposition reaction, but in the temperature range from 800 to 3,000 k, the branching ratio of channel (4) decreases gradually from 99.90 to 89.20%, while that of CH_3COH [channel (5)] increases gradually from 0.13 to 4.65%. The branching ratio of CH_2CHO + H [channel (6)] increases gradually from 0.33% at 1,200 k to 5.60% at 3,000 k.

4 Conclusion

For the unimolecular decomposition of *syn*-vinyl alcohol, chemically accurate ab initio CCSD(T)/6-311 + G(3df, 2p)//B3LY/6-311G(d,p) calculation of PES is performed. The rate constants for the decomposition of *syn*-vinyl alcohol are computed with a microcanonical RRKM and VTST method using the Variflex code. The results calculated show that the decomposition of *syn*-vinyl alcohol to CH_3 + CHO products via the isomerization intermediate CH_3CHO [channels (4)] is dominant, and its product branching ratio at 0.1, 1.0, and 100.0 atm are more than 99.90%, 99.30%, and 89.20%, respectively, through the whole temperature range from 500 to 3,000 K. The fragmentation reactions producing CH_2COH + H (1) and

$CH_2CHO + H$ (6), the H_2O elimination processes producing $CH_2C + H_2O$ (2) and $CHCH + H_2O$ (3) as well as the isomerization process producing CH_3COH (5) are found to be unimportant throughout the temperature and pressure ranges investigated with a maximum branching ratio less than 5.60%. So the unimolecular decomposition of *syn*-vinyl alcohol to CH_3 and HCO products via the isomerization intermediate CH_3CHO is more favorable than the other five channels due to its lower barrier. We fit the rate constants for channels (1)–(6) in temperature and pressure ranges investigated to a modified three-parameter Arrhenius expression, in which the rate constant for channel (4) is $k(CH_3 + HCO) = 4.42 \times 10^{42}\ T^{-9.09}\ \exp(-33{,}754/T)\ s^{-1}$ in the temperature range from 500 to 3,000 K at atmospheric pressure.

The rate constants for the present reaction computed with ab initio molecular orbital and RRKM method are expected to be of high accuracy. They can be included in the existing kinetic schemes for modeling of hydrocarbon flame combustion and can improve the prediction of enols.

Acknowledgments This work has been supported by the National Natural Science Foundation of China (Nos. 91016002, 20973118) and by the Natural Science Foundation of the Education Department of Sichuan Province in China (No.09ZA144).

References

1. Erlenmeyer E (1880) Chem Ber 13:305
2. Saito S (1976) Chem Phys Lett 42:399
3. Toullec J, El-Alaoui MJ (1986) Org Chem 51:4054
4. Capon B, Guo BZ, Kwok FC, Siddhanta AK, Zucco C (1988) Acc Chem Res 21:135
5. Hart H (1979) Chem Rev 79:515
6. Senosiain JP, Klippenstein SJ, Miller JA (2006) J Phys Chem A 110:6960
7. Chandra AK, Thérèse ZH (2003) J Org Chem 68:3618
8. Smith BJ, Nguyen MT, Bouma WJ, Radom L (1991) J Am Chem Soc 113:6452
9. Cool TA, Nakajima K, Mostefaoui TA, Qi F, McIlroy A, Westmoreland PR, Law ME, Poisson L, Peterka DS, Ahmed M (2003) J Chem Phys 119:8356
10. Taatjes CA, Hansen N, McIlroy A, Miller JA, Senosiain JP, Klippenstein SJ, Qi F, Sheng L, Zhang Y, Cool TA, Wang J, Westmoreland PR, Law ME, Kasper T, Kohse-Höinghaus K (2005) Science 308:1887
11. Yamada T, Bozzelli JW, Lay T (1999) J Phys Chem A 103:7646
12. Hippler H, Viskolcz B (2000) Phys Chem Chem Phys 2:3591
13. Taatjes CA, Hansen N, Miller JA (2006) J Phys Chem A 110:3254
14. Rodler M, Bauder A (1984) J Am Chem Soc 106:4025
15. Tureček F, Cramer CJ (1995) J Am Chem Soc 117:12243
16. Silva GD, Kim CH, Bozzelli JW (2006) J Phys Chem A 110:7925
17. Becke AD (1992) J Chem Phys 96:2155
18. Becke AD (1992) J Chem Phys 97:9173
19. Lee C, Yang W, Parr RG (1988) Phys Rev B 37:785
20. Hehre W, Radom L, Schleyer PVR, Pople JA (1986) Ab initio molecular orbital theory. Wiley, New York
21. Andersson MP, Uvdal P (2005) J Phys Chem A 109:2937
22. Gonzalez C, Schlegel HB (1989) J Phys Chem 90:2154
23. Raghavachari K, Trucks GW, Pople JA, Head-Gordon G (1989) Chem Phys Lett 157:479
24. Frisch MJ, Trucks GW, Schlegel HB, Scuseria GE, Robb MA, Cheeseman JR, Montgomery JA Jr, Vreven T, Kudin KN, Burant JC, Millam JM, Iyengar SS, Tomasi J, Barone V, Mennucci B, Cossi M, Scalmani G, Rega N, Petersson GA, Nakatsuji H, Hada M, Ehara M, Toyota K, Fukuda R, Hasegawa J, Ishida M, Nakajima T, Honda Y, Kitao O, Nakai H, Klene M, Li X, Knox JE, Hratchian HP, Cross JB, Adamo C, Jaramillo J, Gomperts R, Stratmann RE, Yazyev O, Austin AJ, Cammi R, Pomelli C, Ochterski JW, Ayala PY, Morokuma K, Voth GA, Salvador P, Dannenberg JJ, Zakrzewski VG, Dapprich S, Daniels AD, Strain MC, Farkas O, Malick DK, Rabuck AD, Raghavachari K, Foresman JB, Ortiz JV, Cui Q, Baboul AG, Clifford S, Cioslowski J, Stefanov BB, Liu G, Liashenko A, Piskorz P, Komaromi I, Martin RL, Fox DJ, Keith T, Al-Laham MA, Peng CY, Nanayakkara A, Challacombe M, Gill PMW, Johnson B, Chen W, Wong MW, Gonzalez C, Pople JA (2003) Gaussian 03 (revision B.05)
25. Klippenstein SJ, Wagner AF, Dunbar RC, Wardlaw DM, Robertson SH (1999) VariFlex version 1.0. Argonne National Laboratory, Argonne
26. Beyer T, Swinehart DF (1973) Commun Assoc Comput Mach 16:379
27. Stein SE, Rabinovitch BS (1973) J Phys Chem 58:2438
28. Gilbert RG, Smith SC (1990) Theory of unimolecular and recombination reactions. Blackwell, Carlton
29. Holbrook KA, Pilling MJ, Robertson SH (1996) Unimolecular reactions. Wiley, New York
30. Miller JA, Klippenstein SJ (2003) J Phys Chem A 107:2680
31. Miller JA, Klippenstein SJ, Raffy C (2002) J Phys Chem A 106:4904
32. Miller JA, Klippenstein SJ, Robertson SH (2000) J Phys Chem A 104:7525
33. Fernandez-Ramos A, Miller J, Klippenstein S, Truhlar D (2006) Chem Rev 106:4518
34. Miller J, Klippenstein S (2006) J Phys Chem A 110:10528
35. Zhou CW, Li ZR, Liu CX, Li XY (2008) J Chem Phys 129:234301
36. Park J, Zhu RS, Lin MC (2002) J Chem Phys 117:3224
37. Matti GY, Osman OI, Upham JE, Suffolk RJ, Kroto HW (1989) J Electron Spectrosc Relat Phenom 49:195
38. Rodler M (1985) J Mol Spectrosc 114:23
39. Bouma WJ, Adom L (1978) J Mol Struct 43:267
40. Yasunaga K, Kubo S, Hoshikawa H, Kamesawa T, Hidaka Y (2008) Int J Chem Kinet 40:73
41. Gupte KS, Kiefer JH, Tranter RS, Klippenstein SJ, Harding LB (2007) Proc Combust Inst 31:167
42. Bentz T, Striebel F, Olzmann M (2008) J Phys Chem A 112:6120
43. Horowltz A, Calvert JG (1982) J Phys Chem 86:3105
44. Joshi A, You XQ, Barckholtz TA, Wang H (2005) J Phys Chem A 109:8016
45. Yadav JS, Goddard JD (1986) J Chem Phys 84:2682
46. Nilsson EJK, Bache-Andreassen L, Johnson MS, Nielsen CJ (2009) J Phys Chem A 113:3498
47. Harding LB, Georgievskii Y, Klippenstein SJ (2010) J Phys Chem A 114:765
48. Tardy DC, Rabinovitch BS (1977) Chem Rev 77:369
49. Quack M, Troe J (1977) In: Asmore PG, Donovan RJ (eds) Gas kinetics and energy transfer, vol 2. The Chemical Society, London
50. Poling BE, Prausnitz JM, O'Connell JP (2001) The properties of gases and liquids, 5th edn. McGraw-Hill, New York
51. Mourits FM, Rummens HA (1977) Can J Chem 55:3007
52. Zhu RS, Lin MC (2004) Chem Phys Chem 5:1864
53. Eckart C (1930) Phys Rev 35:1303